Hot-electron dynamics and terahertz generation in GaN quantum wells in the streaming transport regime

J. T. Lü,* J. C. Cao,† and S. L. Feng

State Key Laboratory of Functional Materials for Informatics, Shanghai Institute of Microsystem and Information Technology, Chinese Academy of Sciences, 865 Changning Road, Shanghai 200050, People's Republic of China

(Received 12 August 2005; revised manuscript received 31 October 2005; published 25 May 2006)

We study hot-electron transport and the dynamic negative differential conductivity in a GaN/AlGaN quantum well by using the Monte Carlo method. We find that the electron-electron interaction, the nonequilibrium polar optical phonon, and the electron gas degeneracy may influence the electron transport property and destroy the spindle-shaped distribution in the streaming transport regime. Our simulation results suggest that the hot phonon effect, and the electron gas degeneracy are more important in the determination of electron steady state velocity-field characteristics, while the electron-electron interaction is dominant in the disturbance of the electron periodic motion. We conclude that terahertz generation using the electron dynamic negative differential conductivity is only possible at relatively low electron density before the electron-electron interaction steps into role.

DOI: 10.1103/PhysRevB.73.195326 PACS number(s): 73.63.Hs, 63.20.Kr, 72.30.+q, 72.20.Ht

I. INTRODUCTION

Recent progress in material growth and device processing techniques[1–4] makes possible the realization of a number of nitride based devices.[5–13] Among them is the widely discussed sub-terahertz (THz) and THz[14] maser utilizing electron instabilities in the streaming transport regime.[8–13,15–19] The high frequency signal generation is associated with the periodic motion of electrons in the momentum space under a constant electric field. At low temperature, the probability of optical phonon absorption is practically negligible. Under a suitable electric field, the momentum relaxation time due to acoustic phonons and ionized impurities is much larger than the time needed for an electron to gain the energy of one polar optical phonon. Moreover, it is much smaller than the relaxation time due to polar optical phonon emission. In this case, electron motion in the momentum space can be divided into two different regions: the so called passive and active regions.[13,15–20] Their boundary corresponds to the threshold momentum value of polar optical phonon emission. In the passive region, electrons are accelerated nearly ballisticly due to low scattering rates with acoustic phonons, ionized impurities, and the absence of polar optical phonon emission. As soon as electrons enter into the active region, they are scattered back near the center of passive region via emission of polar optical phonons. Electrons repeat their motion in the passive region. This periodic motion of electrons in the passive region leads to a spindle-shaped distribution function strongly elongated along the electric field direction, which is usually called streaming distribution.[20–22] In this streaming transport regime, there arises a dynamic negative differential conductivity (DNDC) due to the nearly periodic motion of electrons in the momentum space.[9,10,13,23] The observation of millimeterwave radiation in *n*-InP at low temperature has confirmed this prediction.[23] In nitrides, this DNDC is enhanced due to their large polar optical phonon energy, strong electron-phonon interaction, and large intervalley energy separation. According to previous studies, the two dimensional electron gas (2DEG) has many advantages for better exploiting the DNDC.[9,10]

The main disadvantage of this effect for high frequency signal generation is the continuous emission of polar optical phonons, which means that a large portion of energy that electrons acquire from electric field transforms to thermal energy. This may also drive polar optical phonons far from their equilibrium distribution. The nonequilibrium phonon distribution consequently modifies the electron-phonon interaction. This makes the reabsorption of phonons possible at a high rate, and consequently destroys the phase coherence of the electron motion. So hot phonons exist in large numbers and need to be taken into account. On the other hand, due to the large concentration of 2DEG in nitrides, the electron-electron (e-e) interaction may also play an important role. At the same time, for large electron concentration, the electron gas degeneracy effect is also important in the hot electron dynamics. The purpose of this paper is to study the influence of the e-e interaction, the hot phonon effect, and the electron gas degeneracy on the hot electron dynamics and the DNDC in the streaming transport regime by using the Monte Carlo[24] (MC) method. Very recently, Ramonas *et al.* have studied hot phonon effect on power dissipation in a biased AlGaN/AlN/GaN channel.[25–27] The theoretical framework used in this paper is similar to that of Ref. 25, except that we take into account the e-e interaction. The Coulombic e-e interaction does not contribute to the power dissipation, but it is rather important in the study of electron DNDC.

II. MONTE CARLO MODEL

Our MC model follows a conventional scheme of an ensemble of particles.[24] Additional to the e-e interaction, electron scatterings with polar optical, acoustic (both piezoelectric and deformation potential coupling), nonpolar optical phonons, and ionized impurities are included. The Pauli exclusion principle is taken into account by using the rejection technique.[28] In the electric field range studied, intervalley phonon scattering is considered negligible, and only the first

three subbands in the Γ valley are taken into account in the simulation. The electron eigenstates and energy band profile are obtained by solving the effective mass Schrödinger and Poisson's equation self-consistently, including the strong spontaneous and piezoelectric polarization field in GaN heterostructures.[29,30]

In uniaxial wurtzite structures, electron-optical-phonon interaction is much more complex than that in cubic structures. But according to recent studies, the expression of longitudinal optical (LO) phonon scattering rate in cubic structures remains valid in most cases.[25,31] Moreover, we neglect the confinement of optical phonons in the quantum well,[32,33] and use bulk phonon expressions.[34] In the streaming transport regime, the acoustics phonon scattering is an important energy relaxation channel, so we have also taken into account the scattering inelasticity. Following the method in Ref. 34, we get for deformation potential coupling acoustic phonons

$$W_{i,f}(k_i) = \frac{E_a^2 m^*}{4\pi^2\hbar^2\rho v}\int dq_\parallel \int dq_z \frac{H\left[1-\left(\frac{\Delta - q_\parallel^2}{2k_i q_\parallel}\right)^2\right]}{\sqrt{1-\left(\frac{\Delta - q_\parallel^2}{2k_i q_\parallel}\right)^2}} \times \frac{\sqrt{q_\parallel^2+q_z^2}}{k_i}|G_{i\to f}(q_z)|^2\left(N(q)+\frac{1}{2}\pm\frac{1}{2}\right), \quad (1)$$

where

$$G_{i\to f}(q_z) = \int_L dz[\varphi_f(z)^* e^{-iq_z z}\varphi_i(z)], \quad (2)$$

$$\Delta = \frac{2m^*}{\hbar^2}(E_i - E_f \mp \hbar\omega), \quad (3)$$

and φ_i and φ_f are the electron envelope functions of the initial and final states, respectively. E_i and E_f are corresponding eigenenergies. k_i and k_f are the electron momentum value before and after scattering, respectively. $H(x)$ is the step function. E_a is the deformation potential, m^* is the electron effective mass, ρ is the density of the crystal, v is the longitudinal sound velocity, $\hbar$ is the reduced Planck constant, and $\omega = qv$ is the acoustic phonon energy. For piezoelectric coupling acoustic phonons, the scattering rate is

$$W_{i,f}(k_i) = \frac{m^* e^2 K^2 v}{4\pi^2\hbar^2\varepsilon_0\varepsilon_s}\int dq_\parallel \int dq_z \frac{H\left[1-\left(\frac{\Delta - q_\parallel^2}{2k_i q_\parallel}\right)^2\right]}{\sqrt{1-\left(\frac{\Delta - q_\parallel^2}{2k_i q_\parallel}\right)^2}} \times \frac{\sqrt{q_\parallel^2+q_z^2}}{k_i(\sqrt{q_\parallel^2+q_z^2}+q_s)^2}|G_{i\to f}(q_z)|^2\left(N(q)+\frac{1}{2}\pm\frac{1}{2}\right), \quad (4)$$

where K^2 is the electromechanical coupling coefficient whose value is taken from Ref. 35. ε_0 is the permittivity of vacuum, ε_s is the static dielectric constant, and q_s is the inverse screening length. Here the screening effect is ignored, and $q_s = 0$ is used. For the e-e scattering, we use the single subband static screening model. It is valid for the case we study here, since most of the electrons locate in the lowest subband. The scattering rates for an electron in subband i with wave vector $\mathbf{k}_i$ to subband f with wave vector $\mathbf{k}_f$ can be written as[36,37]

$$\Gamma_{if}(k_i) = \frac{e^4 m^*}{16\pi\hbar^3\epsilon^2\epsilon_0 A}\sum_{\mathbf{k}_0,m,n} f_m^{FD}(\mathbf{k}_0)\int_0^{2\pi} d\theta \frac{|F_{imfn}(q)|^2}{(q+q_s)^2}, \quad (5)$$

where $f_m^{FD}(\mathbf{k}_0)$ is the Fermi distribution function of subband m, and

$$F_{imfn}(q) = \int dz \int dz' \varphi_n^*(z')\varphi_f^*(z)\varphi_i(z)\varphi_m(z')\exp(-q|z-z'|), \quad (6)$$

$$(2q)^2 = 2g^2 + \Delta k_0^2 - 2g\sqrt{g^2+\Delta k_0^2}\cos\theta, \quad (7)$$

$$\Delta k_0^2 = \frac{4m^*}{\hbar^2}(E_i + E_m - E_f - E_n), \quad (8)$$

$$\mathbf{g} = \mathbf{k}_0 - \mathbf{k}_i, \quad (9)$$

$$\mathbf{g}' = \mathbf{k}_0' - \mathbf{k}_f. \quad (10)$$

The e-e scattering is a dual-particle process. During the process, another electron initially in subband m with wave vector $\mathbf{k}_0$ is scattered to subband n with wave vector $\mathbf{k}_0'$. θ is the angle between $\mathbf{g}$ and $\mathbf{g}'$. The quasi-2D inverse screening length q_s in the single subband static screening approximation is

$$q_s = \frac{m^* e^2}{2\pi\epsilon_0\epsilon\hbar^2}n_{1,\mathbf{k}=0}. \quad (11)$$

Here, $n_{1,\mathbf{k}=0}$ is the electron distribution function when $\mathbf{k}=0$. The e-e scattering rates are included into the MC procedure by following the method of Ref. 36.

To fully take into account the 2D nature, we use the rejection technique for the determination of states after scattering. According to the transition probability expressions, we compute the in-plane angle dependence of each scattering mechanism and store the information in a look-up table. During scattering, we check this table and compute the scattering probability for each angle via linear interpolation. Finally, the scattering angel is determined by using the rejection technique.

Hot phonon dynamics can be incorporated into the MC procedure by using the relaxation time approximation.[25,40,43,44] The time evolution of the polar optical phonon population is followed, and its modification to electron-phonon interaction is considered. The LO phonon decay into other modes is taken into account by introducing the relaxation time τ_{ph}, which is taken to be 1 ps.[41] In detail, the perpendicular component q_z is tabulated for discrete values corresponding to intra- and inter-subband transitions, respectively. It is zero for intrasubband transitions, and is a nonzero

TABLE I. Material parameters used in the simulation.

Parameters	Unit	GaN Value	AlGaN value
Effective mass	m_0	0.212	$0.252x+0.228$
Static dielectric constant	ϵ_0	9.5	$-0.3x+10.4$
Optical dielectric constant	ϵ_0	5.35	
Energy Bandgap (E_g)	eV	3.42	$6.13x+3.42(1-x)-x(1-x)$
Energy Barrier	eV	0	$0.7[E_g(x)-E_g(0)]$
LO phonon energy	meV	92	
Mass density	$\times 10^3$ kg/cm^3	6.095	
Sound velocity	$\times 10^3$ m/s	6.6	
Acoustic deformation potential	eV	8	
Pieoelectric constants	C/m^2	$e_{15}=-0.49$	
		$e_{31}=-0.33$	
		$e_{33}=0.7$	
Elastic constants	$\times 10^{11}$ N/m^2	$c_{\mathrm{LA}}=2.65$	
		$c_{\mathrm{TA}}=0.442$	
Electromechanical coupling coefficient	arb. units	0.039	

value related to the subband energy difference for intersubband transitions. The in-plane component of the phonon wave vector $q_{\|}$ is treated as two dimensional, and is discretized into small cells. The phonon number in each cell is initialized as the Bose distribution. After each LO phonon emission (absorption), their values are updated in the corresponding cell as

$$\delta N_q = \pm \left(\frac{2\pi}{\delta q_x}\right)\left(\frac{2\pi}{\delta q_y}\right)\left(\frac{n_s}{N}\right). \tag{12}$$

Here δq_x and δq_y are the cell size in x and y directions, respectively, n_s is the electron sheet density, and N is the number of particles included in the MC simulation. At the end of each time interval, the phonon number is recalculated as

$$N_q'(i\delta t) = N_q(i\delta t) - [N_q(i\delta t) - N_q(0)]\frac{\delta t}{\tau_{ph}}, \tag{13}$$

where δt is the time interval in the MC simulation, which is chosen to be much smaller than τ_{ph}.

We study a GaN quantum well with width $d=8$ nm, which is surrounded by two $Al_{0.4}Ga_{0.6}N$ barriers. The structure is 5 nm planar doped from each boundary. In this configuration, the energy separation between the two lowest subbands is greater than the polar optical phonon energy so that most of the electrons locate in the first subband during their quasiballistic motion. Different doping densities are taken into account in the present paper, since hot phonon population depends heavily on electron concentration. Other material parameters are taken from Refs. 38 and 39, and are listed in Table I.

III. THE ELECTRON-ELECTRON INTERACTION, THE HOT PHONONS, AND THE ELECTRON GAS DEGENERACY

In this section, we compare the influence of the e-e interaction, the hot phonons, and the electron gas degeneracy on the electron velocity-field characteristics. In Fig. 1, we show the electron velocity-field characteristics under electric fields below 30 kV/cm at 4.2 and 300 K under different cases. The electron sheet density is taken to be 1×10^{12} cm^{-2}. We can

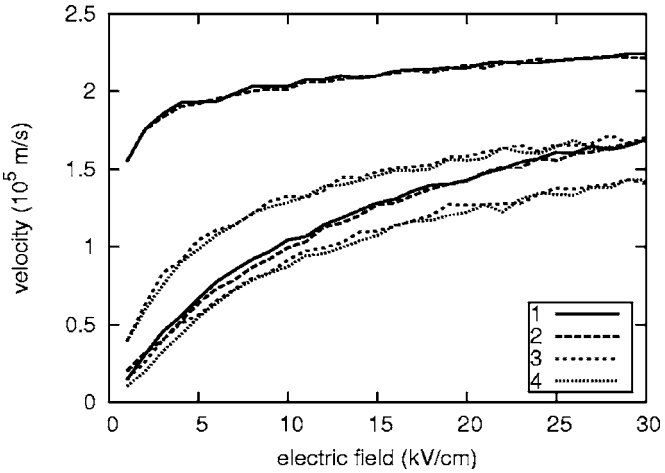

FIG. 1. Electron velocity-field characteristics for the structure studied under different circumstances. The temperature of the lower four curves is 4.2 K, and others 300 K. (1) Without the hot phonon effect, the e-e interaction, and the electron gas degeneracy, (2) with the electron gas degeneracy, but without the e-e interaction, and the hot phonon effect, (3) with the electron gas degeneracy, and the hot phonon effect, but without the e-e interaction, (4) with all of the three mechanisms. The population of hot phonons decreases electron drift velocity, but the e-e interaction, and the electron gas degeneracy have little effect.

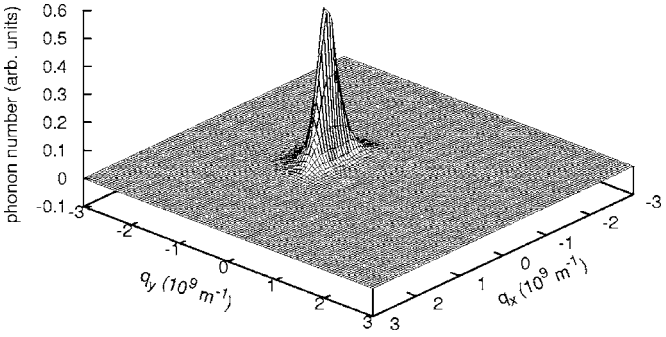

FIG. 2. Nonequilibrium phonon distribution under the electric field of 10 kV/cm at 4.2 K. The electron sheet density is 1×10^{11} cm^{-2}. It is symmetric with respect to the q_x direction, and shifted in the direction opposite to the electric field.

see that the hot phonon effect has the most significant influence on the electron drift velocity. It gets much lower when the hot phonon effect is included. Meanwhile, this decrease at lower temperature is much larger than that at higher temperature. On the other hand, the e-e interaction and the electron gas degeneracy have little effect on the electron drift velocity under the circumstances we study here. We can see that turning on or off the e-e interaction, and the electron gas degeneracy only changes the velocity-field characteristics slightly. This is true whether or not we take into account the hot phonon effect. The e-e interaction is elastic, and it only helps to exchange energy among electrons and does not change the total energy of the electron system at all. From this point of view, we can say that it is reasonable for Ref. 25 to neglect the e-e interaction in the study of energy dissipation in GaN 2DEG. In what follows, we can see that the e-e interaction plays an important role in disturbing the phase coherence, and destroying the DNDC in the electron motion. The electron gas degeneracy is a rather different case. Though it is not important in the cases we study here, the electron gas degeneracy will play an important role in the determination of the electron velocity-field characteristics when the electron sheet density is high enough. Indeed we have performed many such simulations. We find that when the electron sheet density is several 10^{12} cm^{-2}, the electron gas degeneracy will make the electron drift velocity much lower. These results are consistent with those in Ref. 27.

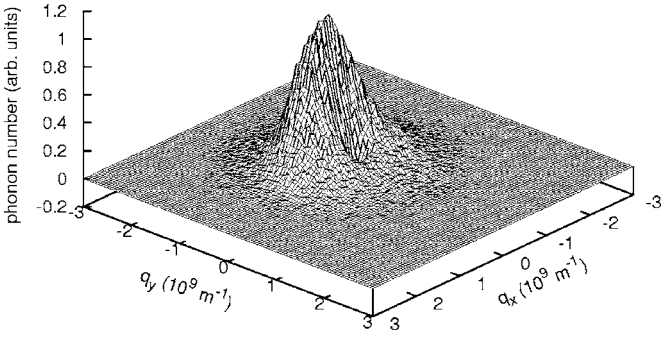

FIG. 3. Nonequilibrium phonon distribution at the electron sheet density of 1×10^{12} cm^{-2}. Other parameters are the same as Fig. 2. Hot phonons distribute in a much larger momentum space than in Fig. 2.

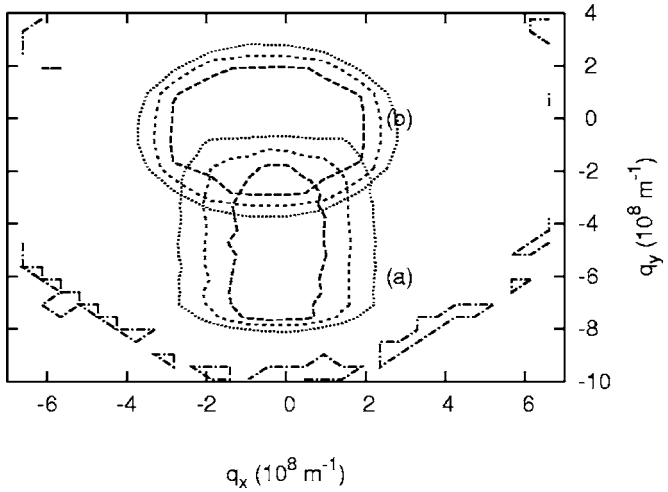

FIG. 4. Contour plot of electron distribution in the momentum space under the electric field of 10 kV/cm at 4.2 K. The electron sheet density is 1×10^{12} cm^{-2}. The electron gas degeneracy is taken into account. (a) Spindle-shaped, without hot phonons; (b) circular-shaped, with hot phonons. Beginning from the smallest, the closed contour lines represent values of 0.6, 0.4, 0.2, respectively.

Now we study the hot phonon distribution under different electron concentration without taking into account the e-e interaction. In Figs. 2 and 3, we show the nonequilibrium phonon distribution for the structure studied under a constant electric field of 10 kV/cm applied in y direction. The temperature is 4.2 K. The sheet electron densities are 1×10^{11} and 1×10^{12} cm^{-2}, respectively. At lower electron concentration (Fig. 2), the influence of nonequilibrium phonons is not significant. Electrons move periodically in the passive region, and emit LO phonons with similar wave vectors. Nonequilibrium phonons are populated only in a small region of the quasimomentum space. The distribution is symmetrical with respect to the q_x axis, and shifted in the direction opposite to the electric field. For a larger electron concentration (Fig. 3), hot phonons are populated in a much larger quasimomentum space, and their value gets larger. Reabsorption of previous emitted phonons is more likely to happen, which randomizes electron phase coherence, and washes out the peak appearing at lower concentration. The randomization of phonon wave vector makes the coupled electron distribution more isotropic, and destroys the transit time resonance in their motion. Limited by the energy and momentum conservation laws, there is a quasicircular region around $|q_{\|}|=0$ where the phonon population remains at equilibrium value.

When the electron sheet density is 1×10^{12} cm^{-2}, the hot phonon effect is strong enough to destroy the phase coherence of electron motion at low temperature. As an example, we depict the contour plot of electron distribution in the momentum space under an electric field of 10 kV/cm in Fig. 4. In the absence of the hot phonon effect, electrons form a spindle-shaped distribution, which is the essential condition for the appearance of DNDC. If hot phonons are taken into account, their nonequilibrium population modifies electron-phonon interaction. The optical phonon absorption rates dramatically increase for some phonon wave vectors. Electrons have a large possibility to absorb the emitted phonons, which

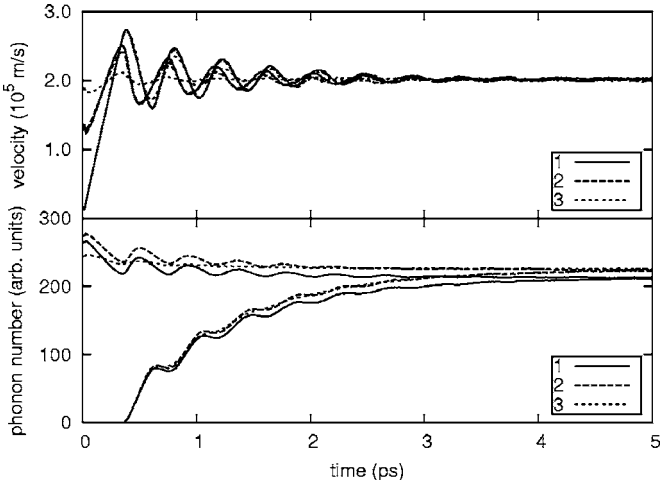

FIG. 5. Transient time evolution of the electron drift velocity (top), the hot phonon number (bottom), and their responses upon an impulse perturbation under different circumstances. The electron sheet density is 1×10^{11} cm^{-2}. (1) Without the e-e interaction, and the electron gas degeneracy, (2) without the e-e interaction, with the electron gas degeneracy, (3) with both the e-e interaction, and the electron gas degeneracy.

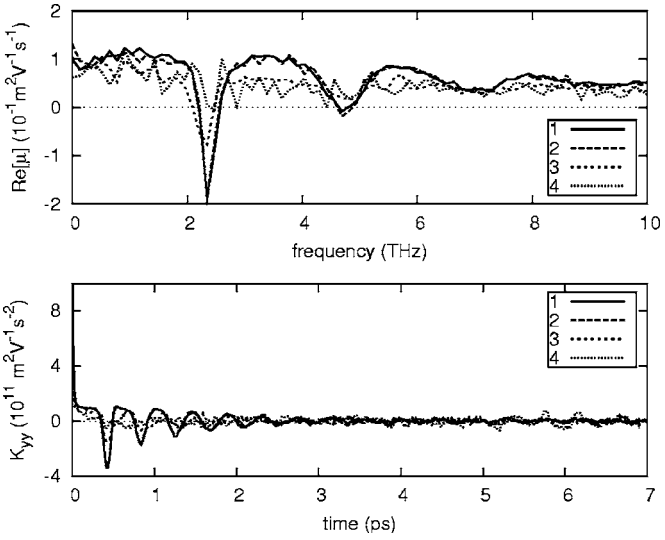

FIG. 6. (bottom) The time response function K_{yy} of the electron drift velocity. (top) Real part of the electron differential mobility Re[μ_{yy}]. The electron sheet density is 1×10^{11} cm^{-2}. (1) Without the e-e interaction, the hot phonon, and the electron gas degeneracy effect, (2) without the e-e interaction, the hot phonon effect, but with the electron gas degeneracy, (3) with the hot phonon effect, and the electron gas degeneracy, but without the e-e interaction, (4) with the e-e interaction, and the electron gas degeneracy, but without the hot phonon effect.

will destroy the phase coherence. In this case, electrons form a nearly circular distribution in the momentum space [Fig. 4(b)].

IV. DYNAMIC NEGATIVE DIFFERENTIAL CONDUCTIVITY AND TERAHERTZ GENERATION

In this section, we study the time response of electron longitudinal velocity on impulse perturbation, and the electron differential mobility spectra using the method proposed in Ref. 42. To study the relative importance of different mechanisms, we set the electron sheet density to 1×10^{11} cm^{-2}. Figure 5 demonstrates the transient evolution of electron drift velocity, hot phonon number, and their responses upon an impulse perturbation, with and without the e-e interaction, and the electron gas degeneracy, respectively. Both electrons and phonons are driven away from quasiequilibrium by the impulse perturbation and restore their stationary states after relaxation of several picoseconds. The time needed for phonons to reach their quasiequilibrium state is a little larger than that of electrons. In cases without the e-e interaction, the phonon replica are well resolved, which indicates the periodic emission of hot phonons when electrons reach their threshold energy. In the presence of e-e interaction, those phonon replicas are not so obvious, which indicates the destroying of periodic emission of hot phonons by e-e interaction. Due to the relatively low electron concentration, the electron gas degeneracy slightly modifies the transient evolution of hot electrons and phonons. This modification is much weaker than that of the e-e interaction. So at relatively low electron concentrations the e-e interaction will dominate over other mechanisms in destroying the electron periodic motion in the passive region.

For the sake of clarity, we show the time response function of drift velocity upon small signal perturbation in the lower part of Fig. 6. Without the hot phonon effect, and the e-e interaction, it decreases abruptly at first, and then enters into damped periodic oscillation around zero. The oscillation period is about 0.4 ps, which corresponds to the time that electrons need to reach the boundary of the passive region, and the period of phonon replica in Fig. 5. The electron gas degeneracy has little effect on this behavir. In the presence of hot phonon effect, the amplitude of the damping oscillation gets smaller. Furthermore, if we turn on the e-e interaction, this oscillation behavior is destroyed. We can get the differential mobility spectra by Fourier transforming the time response function K_{yy} as

$$\mu_{yy}(\omega) = \int_0^\infty K_{yy}(t)e^{-i\omega t}dt. \tag{14}$$

The upper part of Fig. 6 shows the real part of the longitudinal differential mobility Re[μ_{yy}], which exhibits a series of resonances at the transit-time frequency and its higher harmonics. The fundamental resonance is the strongest. The higher resonances get weaker and weaker. The first minimum of the resonances is negative, which means the appearance of DNDC. The small DNDC band can be used for THz signal generation. The narrow band is favorable for single mode operation. We can see that the electron gas degeneracy has little effect on the electron DNDC under the electron concentration studied. When we include the hot phonon effect, the value of DNDC peaks gets smaller, but still available. Meanwhile, in the presence of the e-e interaction, the DNDC peaks disappear. The e-e interaction destroys the electron periodic motion and the DNDC before the hot phonon effect, and the

electron gas degeneracy step into roles. Among the three mechanisms, the e-e interaction is the most criminal one. So the realization of THz maser using the electron DNDC is only possible when the electron concentration in the 2DEG is low enough where the e-e interaction does not step into role.

V. CONCLUSIONS

In conclusion, the influence of the e-e interaction, the hot phonon effect, and the electron gas degeneracy on the electron periodic motion and THz generation in a GaN/AlGaN quantum well is studied by using the MC method. Two dimensional nature of the scattering is taken into account via the rejection technique. For relatively low electron concentration, the e-e interaction is stronger than the hot phonon, and the electron gas degeneracy effect in destroying the electron periodic motion and DNDC, though it has little effect on the electron velocity-field characteristics. At large electron concentrations, all of the three mechanisms contribute to the disturbance of electron phase coherence, and thus destroy the DNDC. So the realization of a THz maser is only possible when the electron concentration in the 2DEG is low enough where the e-e interaction does not step into role.

ACKNOWLEDGMENTS

This work was supported by the National Fund for Distinguished Young Scholars of China (60425415), the major project of the National Science Foundation of China (10390162), and the Shanghai Municipal Commission of Science and Technology. One of the authors (J.T.L.) would like to thank Dr. X. G. Guo for simulation discussions.

*Electronic address: tower.lu@gmail.com
†Electronic address: jccao@mail.sim.ac.cn

[1] C. Skierbiszewski, K. Dybko, W. Knap, M. Siekacz, W. Krupczynski, G. Nowak, M. Bockowski, J. Lusakowski, Z. R. Wasilewski, and D. Maude *et al.*, Appl. Phys. Lett. **86**, 102106 (2005).
[2] E. Frayssinet, W. Knap, P. Lorenzini, N. Grandjean, J. Massies, C. Skierbiszewski, T. Suski, I. Grzegory, S. Porowski, and G. Simin *et al.*, Appl. Phys. Lett. **77**, 2551 (2000).
[3] M. J. Manfra, N. G. Weimann, J. W. P. Hsu, L. N. Pfeiffer, K. W. West, S. Syed, H. L. Stormer, W. Pan, D. V. Lang, and S. N. G. Chu *et al.*, J. Appl. Phys. **92**, 338 (2002).
[4] T. Wang, Y. Ohno, M. Lachab, D. Nakagawa, T. Shirahama, S. Sakai, and H. Ohno, Appl. Phys. Lett. **74**, 3531 (1999).
[5] Y. Deng, R. Kersting, J. Xu, R. Ascazubi, X.-C. Zhang, M. S. Shur, R. Gaska, G. S. Simin, M. A. Khan, and V. Ryzhii, Appl. Phys. Lett. **84**, 70 (2004).
[6] V. D. Jovanović, D. Indjin, Z. Ikonić, and P. Harrison, Appl. Phys. Lett. **84**, 2995 (2004).
[7] J. T. Lü and J. C. Cao, Semicond. Sci. Technol. **19**, 451 (2004).
[8] E. A. Barry, K. W. Kim, and V. A. Kochelap, Appl. Phys. Lett. **80**, 2317 (2002).
[9] K. W. Kim, V. V. Korotyeyev, V. A. Kochelap, A. A. Klimov, and D. L. Woolard, J. Appl. Phys. **96**, 6488 (2004).
[10] V. V. Korotyeyev, V. A. Kochelap, K. W. Kim, and D. L. Woolard, Appl. Phys. Lett. **82**, 2643 (2003).
[11] E. Starikov, P. Shiktorov, V. Gružinskis, L. Reggiani, L. Varani, J. C. Vaissire, and J. H. Zhao, IEEE Trans. Electron Devices **48**, 438 (2001).
[12] E. Starikov, P. Shiktorov, V. Gružinskis, L. Reggiani, L. Varani, J. C. Vaissiére, and J. H. Zhao, J. Phys.: Condens. Matter **13**, 7159 (2001).
[13] E. Starikov, P. Shiktorov, V. Gružinskis, L. Reggiani, L. Varani, J. C. Vaissiére, and J. H. Zhao, J. Appl. Phys. **89**, 1161 (2001).
[14] J. C. Cao, Phys. Rev. Lett. **91**, 237401 (2003).
[15] G. A. Baraff, Phys. Rev. **128**, 2507 (1962).
[16] G. A. Baraff and S. J. Buchsbaum, Phys. Rev. **130**, 1007 (1963).
[17] G. A. Baraff, Phys. Rev. **133**, A26 (1964).
[18] Y. B. Levinson, JETP Lett. **23**, 697 (1966).
[19] Y. B. Levinson, JETP Lett. **23**, 1104 (1966).
[20] V. Mitin and C. M. Van Vliet, Phys. Rev. B **41**, 5332 (1990).
[21] S. Komiyama, T. Masumi, and K. Kajita, Phys. Rev. Lett. **42**, 600 (1979).
[22] V. V. Mitin, V. A. Kochelap, and M. A. Stroscio, *Quantum Heterostructures* (Cambridge University Press, Cambridge, 1999).
[23] L. E. Vorob'ev, S. N. Danilov, V. N. Tulupenko, and D. A. Firsov, JETP Lett. **73**, 219 (2001).
[24] C. Jacoboni and P. Lugli, *The Monte Carlo Method for Semiconductor Device Simulation* (Springer-Verlag, Wien, New York, 1989).
[25] M. Ramonas, A. Matulionis, J. Liberis, L. Eastman, X. Chen, and Y.-J. Sun, Phys. Rev. B **71**, 075324 (2005).
[26] A. Matulionis, J. Liberis, I. Matulioniene, M. Ramonas, L. F. Eastman, J. R. Shealy, V. Tilak, and A. Vertiatchikh, Phys. Rev. B **68**, 035338 (2003).
[27] M. Ramonas, A. Matulionis, and L. Rota, Semicond. Sci. Technol. **18**, 118 (2003).
[28] P. Lugli and D. K. Ferry, IEEE Trans. Electron Devices **32**, 2431 (1985).
[29] V. Fiorentini, F. Bernardini, A. D. C. Fabio Della. Sala, and P. Lugli, Phys. Rev. B **60**, 8849 (1999).
[30] J. M. Li, Y. W. Lü, D. B. Li, X. X. Han, Q. S. Zhu, X. L. Liu, and Z. G. Wang, J. Vac. Sci. Technol. B **22**, 2568 (2004).
[31] C. Bulutay, B. K. Ridley, and N. A. Zakhleniuk, Phys. Rev. B **62**, 15754 (2000).
[32] J. T. Lü and J. C. Cao, Phys. Rev. B **71**, 155304 (2005).
[33] J. T. Lü and J. C. Cao, J. Appl. Phys. **97**, 033502 (2005).
[34] P. Kinsler, Tech. Rep., Imperial College, Prince Consort Road, London SW7 2BZ, United Kingdom (2002).
[35] B. K. Ridley, B. E. Foutz, and L. F. Eastman, Phys. Rev. B **61**, 16862 (2000).
[36] S. M. Goodnick and P. Lugli, Phys. Rev. B **37**, 2578 (1988).
[37] M. Mosko, A. Mosková, and V. Cambel, Phys. Rev. B **51**, 16860 (1995).
[38] T.-H. Yu and K. F. Brennan, J. Appl. Phys. **89**, 3827 (2001).

[39] D. Zanato, S. Gokden, N. Balkan, B. K. Ridley, and W. J. Schaff, Semicond. Sci. Technol. **19**, 427 (2004).

[40] P. Lugli, C. Jacoboni, L. Reggiani, and P. Kocevar, Appl. Phys. Lett. **50**, 1251 (1987).

[41] At room temperature this is a reasonable value, but at 4.2 K its value should be much larger. Due to lack of experimental results at 4.2 K, we take the same value for all temperatures in this paper. So the effect discussed here should be more pronounced at 4.2 K in realistic conditions.

[42] H. Kosina, M. Nedjalkov, and S. Selberherr, J. Appl. Phys. **87**, 4308 (2000).

[43] X. L. Lei and N. J. M. Horing, Phys. Rev. B **35**, 6281 (1987).

[44] W. Cai, M. C. Marchetti, and M. Lax, Phys. Rev. B **34**, 8573 (1986).